

Deformation Behavior of Polyurethane Adhesive in the Single-Lap Joint Based on the Microbeam X-ray Scattering Method

Obayashi, Kakeru
Graduate School of Engineering, Kyushu University

Kamitani, Kazutaka
Institute for Materials Chemistry and Engineering, Kyushu University

Chu, Chien-Wei
Institute for Materials Chemistry and Engineering, Kyushu University

Kawatoko, Ryosuke
Graduate School of Engineering, Kyushu University

他

<https://hdl.handle.net/2324/7172245>

出版情報 : ACS Applied Polymer Materials. 4 (8), pp.5387-, 2022-08-12. American Chemical Society

バージョン :

権利関係 : This document is the Accepted Manuscript version of a Published Work that appeared in final form in The Journal of ACS Applied Polymer Materials, copyright ©2022 American Chemical Society after peer review and technical editing by the publisher. To access the final edited and published work see Related DOI.



1st submission on March 14, 2022

2nd submission on May 23, 2022

3rd submission on June 16, 2022

Deformation behavior of polyurethane adhesive in the single-lap joint based on the microbeam X-ray scattering method

Kakeru Obayashi¹, Kazutaka Kamitani², Chien-Wei Chu²

Ryosuke Kawatoko, Chao-Hung Cheng¹, Atsushi Takahara³, Ken Kojio^{1,2,3,4,5*}

¹Graduate School of Engineering, ²Institute for Materials Chemistry and Engineering, ³Research Center for Negative Emissions Technologies, ⁴International Institute for Carbon-Neutral Energy Research (WPI-I2CNER), ⁵Center for Polymer Interface and Molecular Adhesion Science, Kyushu University, 744 Motoooka, Nishi-ku, Fukuoka 819-0395, Japan

Phone: +81-92-802-2515, Fax: +81-92-802-2518

Keywords: polyurethane; adhesive; microphase-separated structure; small-angle X-ray scattering (SAXS); wide-angle X-ray scattering (WAXS)

*Author to whom correspondence should be addressed.

kojio@cstf.kyushu-u.ac.jp

Abstract

Single-lap joint (SLJ) specimens were prepared using two stainless steel substrates as adherends and polyurethanes (PU) as an adhesive and then employed for adhesion testing. To investigate the internal structure of the PU adhesive during the shear deformation process, the *in situ* synchrotron radiation microbeam small-angle and wide-angle X-ray scattering (SAXS and WAXS) measurements were carried out. A lab-made portable tensile tester was developed for the SAXS/WAXS measurement during lap shear deformation. The structure of adhesive bulk was also investigated during the simple uniaxial deformation for the comparison. An isotropic scattering ring—which was formed from the periodic structure of hard segment domains of the PU adhesive—was clearly observed in the SAXS pattern at the initial state. This isotropic ring changed to an ellipsoid shape whose minor and major axes were tilted from the stretching direction. The spacing of the hard segment domains of PU adhesives increased, and the tilt angle of the stress direction was merged with the stretching direction with an increase in the applied deformation. The orientation direction of the hard segment domains and molecular chain of the soft segment changed with a similar trend. Furthermore, the degree of change in these values was larger at the edge of the adhesive of the SLJ specimens, indicating the existence of spatial distribution of direction and the value of stress in the adhesive during lap shear deformation. These findings are expected to be quite useful for practical design for adhesives.

1. Introduction

In recent years, to reduce the weight of cars and aircrafts, the replacement of metal materials with polymer materials has been promoted to improve fuel efficiency. Using adhesives to bond similar or dissimilar materials together is a potential strategy to fulfill the light weight goal and also has some extra advantages such as good corrosion protection and superior behavior under crashes.¹ The main component of the adhesive is an organic polymer, or one or more compounds that can chemically react and polymerize, which are then cured to a cohesive solid.² However, the detailed principle of adhesion is not completely understood, and problems of safety and reliability still exist. To produce adhesives with high strength and durability, the multi-scale structure must be clarified from the molecular to macroscopic scale of the adhesive. Currently, epoxy, polyurethane (PU), and acrylic resins are the mainly used adhesives in commercial products, and research on their bulk and adhesive properties have been extensively studied in recent years to improve the bonding performance.³⁻⁵

PU is one of the most popular adhesives and generally has a multi-block structure and a microphase-separated structure, in which hard segments form hydrogen bonds and occasionally crystallize. The mechanical and surface properties and the microphase-separated structure of PU can be adjusted by changing the raw materials, polymerization methods, and temperatures.⁶⁻²⁴ Additionally, PU molecules have both polar and non-polar segments, which results in strong adhesion strength between different type of adherends.

The uniaxial deformation behavior of bulk PUs has been investigated using techniques such as birefringence, Fourier transform infrared spectroscopy, small-angle X-ray scattering (SAXS), wide-angle X-ray scattering (WAXS).²⁵⁻³⁰ Recently, with the development of synchrotron radiation facilities, it becomes possible to analyze local structures with microbeams for a short time on the order of milliseconds, and *in situ* structure analysis under deformation has been performed.^{31, 32} Especially, because polymers exhibit relaxation behavior during mechanical testing, *in situ* measurement is

considerably important.

Various testing methods and specimen types have been used for adhesive tests, in which single-lap joint (SLJ) specimen under lap shear deformation is the most commonly used one because of their simple shape and ease of manufacture. Volkersen proposed a model for stress analysis of SLJs, assuming that the adhesive is rigid and deforms only in the shear direction.³³ Goland and Reissner further considered the effects of bending moments on joint ends to make Volkersen's model more applicable to realistic situations.³⁴ Afterwards, the stress distribution inside the adhesive during the deformation process has been evaluated on the micrometer scale by the finite element method (FEM) and digital image correlation (DIC).³⁵⁻³⁸ These pioneering studies showed the regions where stress concentrations were generated in the adhesive layer, and complicated stress fields were formed. However, this has only been understood during changes in the structure of the adhesive in the order of millimeter or sub-millimeter. There is no report on the real stress distribution of adhesive in the SLJ specimens so far. In situ microbeam X-ray scattering measurement can give the strain values through the change in microphase-separated structure of the PU at various positions of adhesive in the SLJ specimen and clarify the stress distribution during the shear deformation process. This finding may be helpful to design strong adhesive and improve for practical applications.

In this study, the changes in the microphase-separated structure of the PU adhesive in SLJ specimens and PU bulk during lap shear and uniaxial deformation processes were analyzed using synchrotron radiation microbeam SAXS and WAXS measurements. Furthermore, the microphase-separated structural changes in lap shear and uniaxial deformation and differences in the structural changes due to stress concentration in the SLJ were discussed.

2. Experimental Section

2.1. Preparation of PU bulk sheet and single-lap joint (SLJ) using PU adhesives

Materials. Poly (oxypropylene) glycol (PPG: number average molecular weight (M_n) = 1000 g mol⁻¹, AGC Inc., Japan), 4,4-diphenylmethane diisocyanate (MDI, Sigma-Aldrich, Japan) and 1,4-butanediol (BD, FUJIFILM Wako Chemical Corporation, Japan) were used as the polymer glycol, diisocyanate, and chain extender. BD was distilled for purification. MDI was used without further purification. Stainless steel (SUS304, length: 30 mm; width: 2 mm; thickness: 1 mm, Yoshikawa seisakujo Corporation, Japan) adherends were washed using hexane, acetone, ethanol, and RO water sequentially with ultrasonication for 10 min and finally exposed to vacuum-ultraviolet (VUV) light for 30 min under reduced pressure.

Sample Preparation. The PPG-MDI-PU was synthesized by a bulk prepolymer method (see in Figure S1(a)). The PPG were first dried under reduced pressure, followed by adding MDI into dry PPG with a formulation ratio of $K = ([NCO]_{iso} / [OH]_{polyol}) = 2.08$ and mixed for 4 h at 80 °C under a nitrogen atmosphere. The extent of the reaction was monitored through an amine equivalent method, and the end of the reaction was determined by confirming that the reaction ratio of NCO groups exceeded 90%. Next, BD was added into the prepolymers with an NCO INDEX = $[NCO]_{pre} / [OH]_{BD}$ of 1.04 and stirred. The product was poured into a mold constructed using a 1 mm thick spacer and two stainless steel plates to form bulk sheet specimens and coated on two SUS304 adherend with the 0.6 mm adhesive thickness to fabricate SLJ specimen. Then, the samples were kept at 120 °C for 24 h. The ratio of mole of MDI : BD : PPG was 2.08 : 1 : 1, and the hard segment content was 37 wt%. The resultant PU is thermoplastic as shown in Figure S2. The method of adjusting adhesive thickness and fixing of sample were the same as those used in our previous study.⁴ The size of the sheet samples used for uniaxial test was 30 mm x 3 mm x 1 mm.

2.2. Microphase-separated structure during two deformation modes *In situ* SAXS and WAXS measurements

The changes in the internal structure of PPG-MDI-PU during tensile deformation and lap shear deformation were investigated by *in situ* SAXS and WAXS measurements at BL05XU beamlines a synchrotron radiation facility in Japan (the SPring-8). The beamline system at BL05XU can provide a microbeam X-rays with a wavelength of 0.1 nm and a beam size of $10\ \mu\text{m} \times 10\ \mu\text{m}$ for precise analyses in microscale regions. For understanding the internal structural changes during uniaxial tensile deformation and lap shear deformation, the corresponding 2D SAXS and WAXS patterns were acquired by irradiating microbeam X-rays passing through 1 mm-thick PU bulk film sheets and SLJ specimens with 2 mm-width adhesive layers with exposure times of 1 ~ 1.5 s, respectively (see Figure 1). The scattered X-rays from the samples were detected for SAXS by a PILATUS 1M detector (DECTRIS Ltd.) with a sample-to-detector distance of 3.88 m and for WAXS by a SOPHIAS detector (RIKEN, Japan) with the distance of 0.11 m. 2D SAXS/WAXS patterns were divided along minor and major axis directions of SAXS/WAXS patterns in lap shear deformation and directions parallel and perpendicular to the elongation direction in uniaxial deformation. The 1D SAXS/WAXS profiles were obtained by integrating 2D SAXS/WAXS patterns using FIT2D software (Andy Hammersley/ESRF). The *in situ* SAXS and WAXS measurements were carried out using a custom-built tensile tester (DIP Co. Ltd.). The tensile rates were 0.5 and 0.01 mm s⁻¹ during uniaxial elongation and lap shear deformation at room temperature, respectively. The shear stress (τ) is defined as the loading force (F) obtained from the tensile tester divided by the overlapping adhesive area (A). The apparent shear strain (γ) was determined based on the displacement recorded from the tensile tester divided by the adhesive thickness.

2.3. Microphase-separated structure during lap shear deformation at various positions

The changes in the internal structures of the PPG-MDI-PU adhesives were investigated at various positions, and cyclic testing was performed. In this test, a fixed shear strain (γ) of 0.5 was imposed on SLJ specimens, and the test was repeated five times. SAXS measurements were performed by passing microbeams through the adhesive at various positions. Five positions were measured to study the positional effect on microphase-separated structure changes, including the positions at the center and 4 corners of the lap-jointed adhesive layer (see Figure S3). Tensile and retraction rates were set at 0.01 mm s⁻¹. The SAXS measurement was performed under the same conditions as those used in section 2.2.

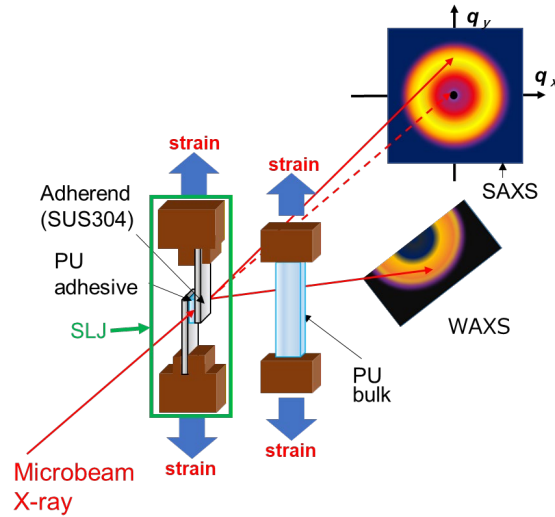


Figure 1. Schematic illustration of the *in situ* SAXS and WAXS measurements of PPG-MDI-PU bulk or SLJ specimens during deformation.

3. Results and Discussion

3.1. Microphase-separated structure changes of bulk PU sheet during uniaxial deformation

Figure 2(a) shows the stress–strain curves obtained during the uniaxial tensile test of the PPG-MDI-PU bulk film. This sample showed rubber-like behavior with more than strain of 8 without fracture. Figure 2(b) shows the SAXS patterns of the PPG-MDI-PU bulk, (c) the corresponding 1D profiles of the meridional and equatorial regions of the PPG-MDI-PU bulk, and (d) the azimuthal angle

profiles of the 2D pattern at $q = 0.20\text{--}1.11\text{ nm}^{-1}$ at various strains. In the SAXS patterns, the direction of the meridional axis corresponded to stretching. The SAXS pattern of PPG-MDI-PU in the initial state exhibited a ring pattern around $q = 0.48\text{ nm}^{-1}$. This ring corresponds to the microphase-separated structure, which consisted of the hard segment domains and a surrounding soft segment matrix. The

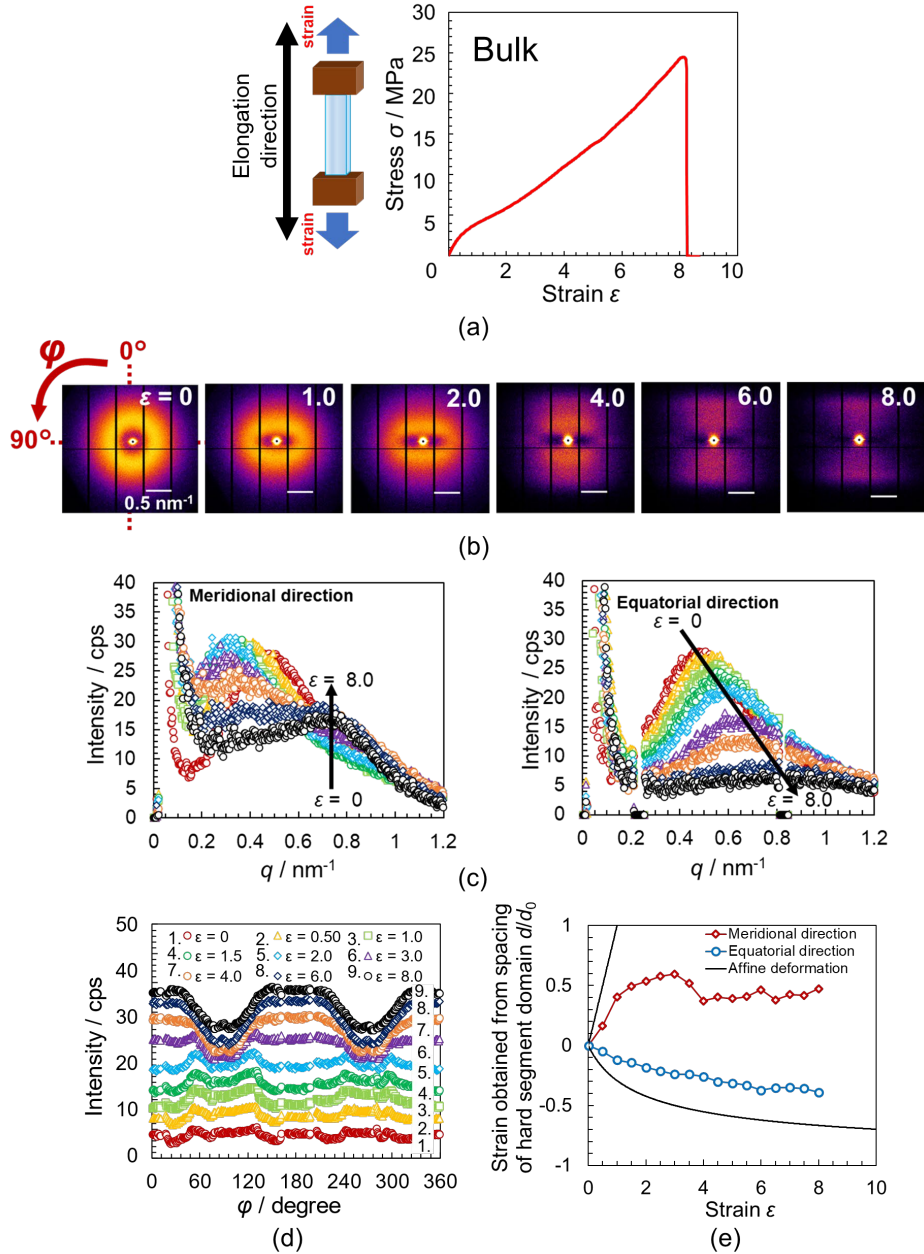


Figure 2. (a) Stress-strain curve of the PPG-MDI-PU bulk during uniaxial deformation. (b) SAXS patterns, (c) 1D meridional and equatorial SAXS profiles, and (d) azimuthal profiles of the SAXS pattern at $q = 0.20\text{--}1.11\text{ nm}^{-1}$ for the PPG-MDI-PU bulk at various strains. (e) strain-strain obtained from spacing of hard segment domain relationship for the PPG-MDI-PU adhesive.

isotropic SAXS pattern in the initial state indicated the hard segment domain was randomly oriented. As the strain increased, this isotropic ring changed to an ellipsoid shape. These results imply that the spacing between hard segment domains parallel to the stress direction (see 1D SAXS results in meridional direction) increased, but the one perpendicular to the stress direction (see 1D SAXS results in equatorial direction) decreased. As shown in Figure 2(d), the four-point scattering pattern was observed in the small ε region, which might be attributable to the anisotropic hard segment microdomains were tilted in this PPG-MDI-PU. In the region of $\varepsilon \geq 3$, the four-point pattern gradually disappeared, and a new scattering pattern appeared around $q = 0.72 \text{ nm}^{-1}$ in the stretch direction. A fan-shaped pattern was observed, and an equatorial intensity distribution occurred because of the curving or undulating of the hard segment domains. These results suggest that the hard segment might be rearranged because of breaking of hard segment domains.³⁹⁻⁴² Desclate scattering was observed on the equatorial line, which corresponds to the formation of bundles. Figures 2 (e) shows relationship between strain obtained from spacing of hard segment domain and film strain of PU bulk during uniaxial deformation. Solid lines correspond to the change in domain spacing when affine deformation occurs. The domain spacing of hard segment domains increased and decreased along the direction of force and the vertical direction to the force with an increase in strain, respectively. Deviation from affine deformation occurred even at small strain. Further, the domain spacing along the force direction stopped increasing at a certain strain. These trends are consistent with obtained for poly(oxytetramethylene) glycol-based PU.²⁹

Figures 3 shows (a) the WAXS patterns, (b) the corresponding 1D-WAXS intensity profile, and (c) the azimuthal angle profiles of the 2D pattern at $q = 11.8\text{--}21.1 \text{ nm}^{-1}$ during elongation for PPG-MDI-PU bulk. At the initial state, a broad halo around $q = 14.2 \text{ nm}^{-1}$ was observed, corresponding to the most probable distance among the molecular chains of soft-soft segments, hard-hard segments and soft-hard segments. In the region of $\varepsilon \geq 3$, the scattering intensity around $q = 13.4 \text{ nm}^{-1}$ in the equatorial

direction increased. The halo derived from the distance between the molecular chains of PPG is observed around $q = 13.2 \text{ nm}^{-1}$ (See Figure S4), and intensity at the equatorial direction showed maximum as shown in Figure 3(c). Thus, the halo around $q = 13.4 \text{ nm}^{-1}$ observed along the equatorial direction can be assigned to the extend PPG.

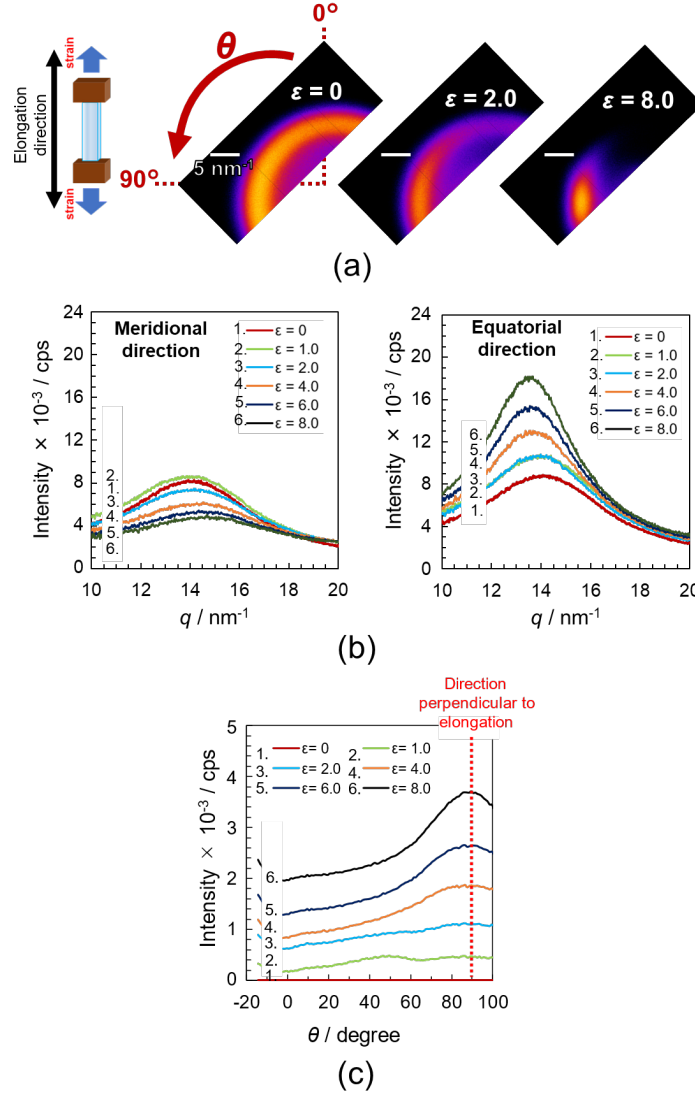


Figure 3. (a) WAXS patterns, (b) 1D meridional and equatorial WAXS profiles, and (c) azimuthal profiles of WAXS pattern at $q = 11.8\text{--}21.1 \text{ nm}^{-1}$ for the PPG-MDI-PU bulk at various strains.

3.2. Microphase-separated structure changes of PU in SLJ during lap shear deformation

Figure 4(a) shows the stress–strain curves during the lap shear test of the PU-SLJ specimen. In the lap shear test, stress increased as the strain increased, and finally, the sample was fractured with

adhesive failure. This SS curve showed a similar trend as that of the bulk. Figure 4 shows (b) the SAXS pattern, (c) the 1D profiles of the PPG-MDI-PU adhesive along the major axis and minor axis direction at various strains, and (d) the azimuthal angle profiles of the 2D pattern at $q = 0.20\text{--}1.11\text{ nm}^{-1}$ during the lap shear test. As the strain increased, this isotropic ring changed to ellipsoid, and the major axis of the ellipsoid declined. These findings imply that the spacing between hard segment domains to the parallel to the macroscopic shear stress direction increased, but that perpendicular to the direction decreased. During the small strain region, same as the bulk, a four-point scattering pattern was observed as shown in Figure 4(d). These scattering intensities were almost the same. In contrast, in $1.5 \leq \gamma \leq 3.5$, the decreasing scattering intensities were observed. As the shear strain increased to $\gamma \geq 3.5$, the four-point pattern gradually disappeared, and a new scattering was observed around $q = 0.72\text{ nm}^{-1}$. Figure S5 shows 1D SAXS profiles of the (a)minor axis and (b)major axis direction at $q = 0\text{--}0.20\text{ nm}^{-1}$ for the PPG-MDI-PU adhesive at various strains. In the high-strain region, streaks were observed at $q \leq 0.20\text{ nm}^{-1}$ in the major axis direction of the elliptical SAXS pattern in SLJ. These findings are considered to be due to the formation of voids or cracks. Comparing with the compressible behavior perpendicular to the strain directions of the bulk PU sheet samples (with a Poisson's ratio of ~ 0.5), that of the PU adhesive of the SLJ samples was restricted due to the bonding between two 2 mm-width adherends, thus voids or cracks are easier to be formed in SLJ than in bulk samples. Figures 4 (e) shows relationship between strain obtained from spacing of hard segment domain and film strain of SLJ specimen during lap shear deformation. The trend is almost the same with that for PU bulk sample shown in Figure 2 (e).

The structure change of crystalline polymers that applied shear deformation have been reported.⁴³⁻
⁴⁵ The following deformation mechanisms are considered for crystalline polymers. The deformation mechanism in the amorphous region of the crystalline polymer before the yielding point is the slip of the chain segment along the axis, similar to the chain slip observed in the crystalline portion of the

polymer. Three transformation modes are envisioned: shearing lamellae of the amorphous phase, and elongation or compression of the tie molecules between lamellae and within their soft amorphous matrix, depending on the original orientation of the lamellae to the applied stress.⁴⁶ There are lamellae

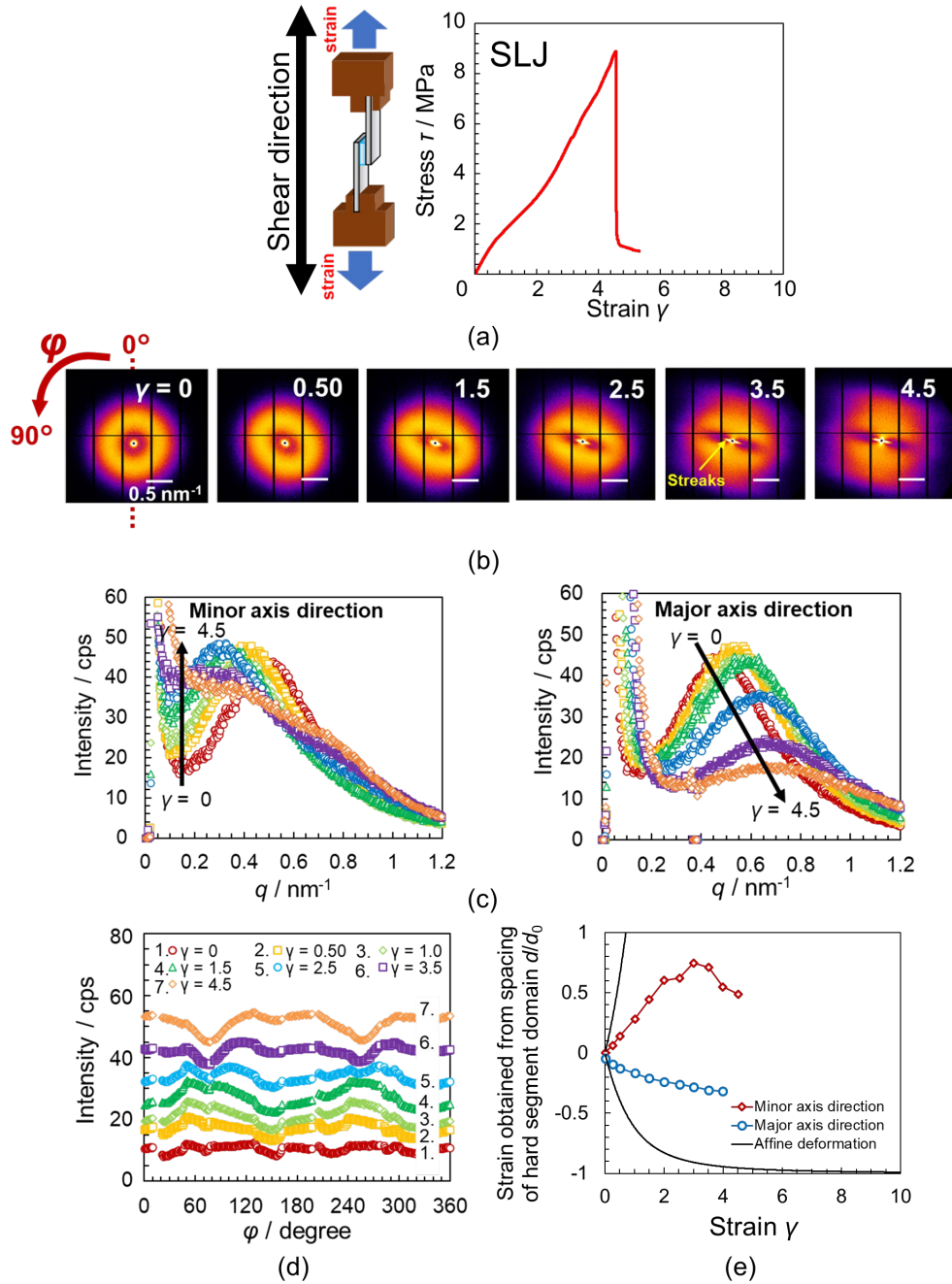


Figure 4. (a) Stress–strain curve of the PPG-MDI-PU adhesive during lap shear deformation. (b) SAXS patterns, (c) 1D SAXS profiles of the minor axis and major axis direction, (d) azimuthal profiles of the SAXS pattern at $q = 0.20$ – 1.11 nm^{-1} , and (e) strain-strain obtained from spacing of hard segment domain relationship for the PPG-MDI-PU adhesive.

with planes orienting all directions, the tie molecules between the lamellae undergo shear deformation until they are completely stretched, after which, the coarse chain slips and lamella block the slide against each other. In contrast, when it is vertical, the tie molecule is subject to volume change; thus, the tie molecule becomes difficult to deform, and a coarse chain slip occurs with a small shear strain. In this paper, they are assumed that lamellae and tie molecules correspond to hard segment domain and soft segment matrix respectively. Therefore, in the case of the PPG-MDI-PU adhesive during lap shear deformation, the soft segment between the hard segment domains parallel to the deformation direction is relatively easily deformed, and the breaking or separation of the hard segment domain is likely to preferentially occur (see Figure S6).

Figures 5 show (a) the WAXS patterns, (b) the corresponding 1D-WAXS intensity profile, and (c) the azimuthal angle profiles of the 2D pattern at $q = 11.8\text{--}21.1\text{ nm}^{-1}$ during lap shear deformation. In the same way as uniaxial deformation, the soft segment chains and hard segment were oriented as the strain increased. It was observed the angle of maximum scattering intensities approached to the shear direction as shown in Figure 5(c). That means that the orientation direction approached to the shear direction. This result indicated that the direction of the orientation of the molecular chain also changed as the direction of the applied force changed.

Figure 6 shows the strain dependence of the orientation direction of the hard segment and soft segment chains obtained from the inclination of the SAXS patterns and the ellipsoid and azimuthal profiles of the WAXS patterns. This rotation angle gradually increased, and the inclination of the ellipse gradually changed so that the minor axis direction approached the tensile direction. These findings clarified that during extension of the single-lap joint sample, the shear stress acted in the oblique direction at the early stage of elongation, and the stress direction gradually changed to the tensile direction side. The directions in domain spacing of hard segment by SAXS and the molecular chains of PU by WAXS, the WAXS showed approximately $2\text{--}3^\circ$ larger angle. This might be because

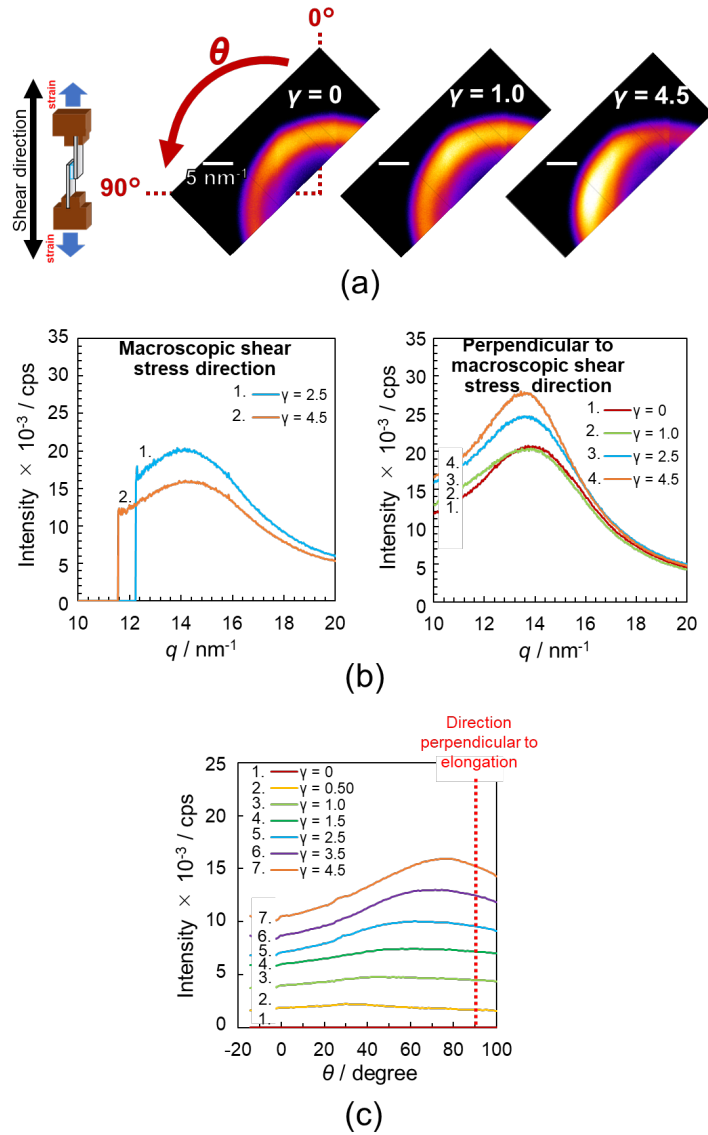


Figure 5. (a) WAXS patterns, (b) 1D WAXS profiles of the macroscopic shear stress and perpendicular to the macroscopic shear stress direction, and (c) azimuthal profiles of the WAXS pattern at $q = 11.8\text{--}21.1 \text{ nm}^{-1}$ for the PPG-MDI-PU adhesive at various strains.

the crystalline hard segment is harder and difficult to be deformed.

The following describes the changing microphase-separated structure of the PPG-MDI-PU adhesive during lap shear deformation (see Figure 7). In the initial state, the PPG-MDI-PU formed the microphase-separated structure without preferential orientation of the hard segment domains. In the region of $\gamma \geq 1.5$, the spacing between hard segment domains parallel to the stress direction increased, but that perpendicular to the stress direction decreased. The orientations of hard segment domains

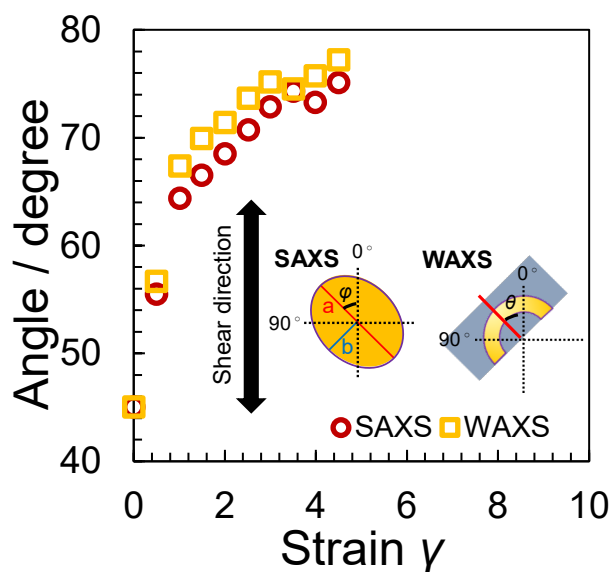


Figure 6. The direction of the change of spacing of hard segment domains and the orientation direction of the molecular chains of PU obtained from the SAXS and WAXS patterns of the PPG-MDI-PU adhesive during lap shear deformation.

inclined the stress direction. The stress direction was tilted from the elongation direction, and the stress direction approached to the tensile direction as the strain increased. In the region of $1.5 \leq \gamma \leq 3.5$, the hard segment domain oriented perpendicular to the deformation direction (Figure S6a) was deformed and broken easily. In contrast, hard segment domain oriented to the deformation direction was hardly deformed and broken (Figure S6b). As the shear strain increased to $\gamma \geq 3.5$, the hard segment domains broke and the orientation direction close to the stress direction. Moreover, voids or cracks might have been occurred.

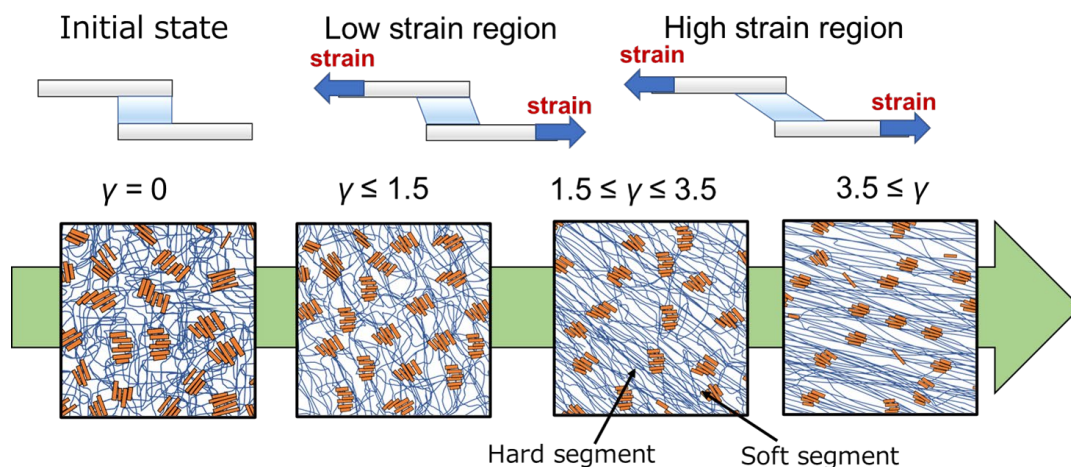


Figure 7. Schematic illustration of the changing microphase-separated structure of the PPG-MDI-PU adhesive during lap shear deformation.

3.3. Microphase-separated structures of PU at various positions of SLJs during lap shear deformation

To clarify the deformation behavior at various positions, the SAXS patterns were obtained at five positions. The same sample was used for these five SAXS measurements. As shown in Figure S7, the decrease in stress by deformation was quite small.

Figure 8 shows the strain dependence of the ellipticity of the SAXS patterns during the cyclic test at five positions. In this experiment, the ellipticity(a/b) of the SAXS patterns was considered to correspond to the magnitude of the internal structural change, where a and b are defined as the lengths in longest and shortest semi-axes of SAXS pattern, respectively. It can be expected that the position measured with a higher ellipticity (a/b) means that PU adhesives were deformed more seriously due to the stronger concentrated stress. From the ellipticity results in Figure 8, it can be found that the micro-scaled deformation in whole adhesive layer was asymmetric and with higher stress concentration at the edge of the adhesive layer (RU and LB positions), middle stress concentration at the center (CC position), minimum at RB and LU positions. Therefore, it is likely that stress concentration occurred at the edge of the adhesive layer. Furthermore, the difference of ellipticity in

the thickness direction shows that the stress distribution was probably anti-symmetrical in thickness direction. In this sample, structural changes were particularly large in LB and RU positions. Figure S8 shows the fillets were formed at the ends of the adherend. That might be the reason of the stress concentration at the edge of adhesive layer. Some group also found the positions of stress concentration if there were fillets in SLJ by FEM (see Figure S9).^{36, 37, 47}

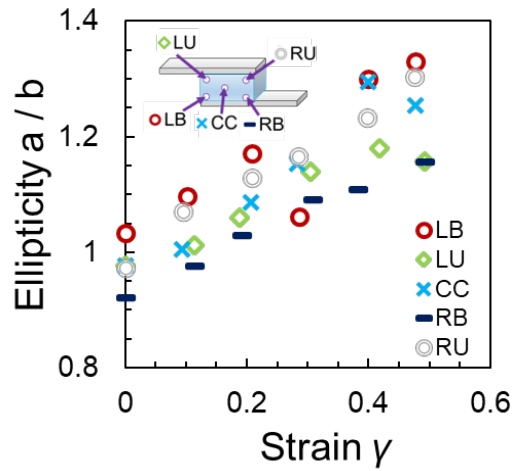


Figure 8. Change in the ellipticity obtained from the SAXS patterns of the PPG-MDI-PU adhesive during cyclic lap shear deformation at five positions. (Ellipticity = the longest semi-axis of ellipsoid a/the shortest semi-axis of ellipsoid b)

4. Conclusions

We performed microbeam SAXS and WAXS measurements, which revealed the changes in the microphase-separated structure of the PPG-MDI-PU adhesive during the deformation processes for both SLJ and bulk specimens. In the tensile shear deformation process, shear stress was applied diagonally from the elongation direction, and the stress direction approached to the tensile direction as the strain increased. In the region of $1.5 \leq \gamma \leq 3.5$, because the intensity ratio of the four-point SAXS pattern changed, it is considered that the flexibility of the soft segment between the hard segment domain differs depending on the orientation direction of the hard segment domain. The hard segment domain oriented perpendicular to the deformation direction was deformed and broken easily. Streaks were observed in the high-strain region of SLJ, suggesting the formation of voids or cracks possibly

due to the restrained deformation of the adhesive by the two adherends. Microbeam SAXS measurements at various positions of SLJ sample revealed the stress distribution in the SLJ adhesive layer, and the maximum stress was applied at the end of adhesive layer. In the future, we expect that this research will lead to better understanding of the adhesive fracture mechanism, thus allowing molecular design of adhesives for increasing the strength of adhesives and the realization of weight reduction in automobiles and aircrafts.

5. Acknowledgments

The research, including the SAXS/WAXS measurements, was supported by the JST Mirai Program (JPMJMI18A2), Japan. SAXS/WAXS data were obtained on BL05XU at the SPring-8 facility with the approval of RIKEN and the Japan Synchrotron Radiation Research Institute (JASRI; Proposal No. 2019A1558). We acknowledge Dr. Taiki Hoshino for his assistance on the SAXS and WAXS measurements.

6. References

1. Pizzi, A.; Mittal, K. L., *Handbook of adhesive technology*. CRC press: 2017.
2. Adams, R. D., *Adhesive bonding: science, technology and applications*. Woodhead Publishing: 2021.
3. Aoki, M.; Shundo, A.; Yamamoto, S.; Tanaka, K., Effect of a heterogeneous network on glass transition dynamics and solvent crack behavior of epoxy resins. *Soft Matter* **2020**, *16* (32), 7470-7478.
4. Chu, C.-W.; Zhang, Y.; Obayashi, K.; Kojio, K.; Takahara, A., Single-Lap Joints Bonded with Epoxy Nanocomposite Adhesives: Effect of Organoclay Reinforcement on Adhesion and Fatigue Behaviors. *ACS Appl. Polym. Mater.* **2021**, *3* (7), 3428-3437.
5. Nguyen, H. K.; Aoki, M.; Liang, X.; Yamamoto, S.; Tanaka, K.; Nakajima, K., Local Mechanical Properties of Heterogeneous Nanostructures Developed in a Cured Epoxy Network: Implications for Innovative Adhesion Technology. *ACS Appl. Nano Mater.* **2021**, *4* (11), 12188-12196.
6. Pandya, M.; Deshpande, D.; Hundiware, D., Effect of diisocyanate structure on viscoelastic, thermal,

- mechanical and electrical properties of cast polyurethanes. *J. Appl. Polym. Sci.* **1986**, 32 (5), 4959-4969.
7. Takahara, A.; Jo, N. J.; Kajiyama, T., Surface molecular mobility and platelet reactivity of segmented poly (etherurethaneureas) with hydrophilic and hydrophobic soft segment components. *J. Biomater. Sci. Polym. Ed.* **1989**, 1 (1), 17-29.
 8. Petrović, Z. S.; Ferguson, J., Polyurethane elastomers. *Prog. Polym. Sci.* **1991**, 16 (5), 695-836.
 9. Nakamae, K.; Nishino, T.; Asaoka, S., Microphase separation and surface properties of segmented polyurethane—Effect of hard segment content. *Int. J. Adhes. Adhes.* **1996**, 16 (4), 233-239.
 10. Nakamae, K.; Nishino, T.; Asaoka, S., Relationships between interfacial properties and structure of segmented polyurethane having functional groups. *Int. J. Adhes. Adhes.* **1999**, 19 (5), 345-351.
 11. Kojio, K.; Uchiba, Y.; Mitsui, Y.; Furukawa, M.; Sasaki, S.; Matsunaga, H.; Okuda, H., Depression of microphase-separated domain size of polyurethanes in confined geometry. *Macromolecules* **2007**, 40 (8), 2625-2628.
 12. Yamasaki, S.; Nishiguchi, D.; Kojio, K.; Furukawa, M., Effects of aggregation structure on rheological properties of thermoplastic polyurethanes. *Polymer* **2007**, 48 (16), 4793-4803.
 13. Tang, Q.; He, J.; Yang, R.; Ai, Q., Study of the synthesis and bonding properties of reactive hot - melt polyurethane adhesive. *J. Appl. Polym. Sci.* **2013**, 128 (3), 2152-2161.
 14. Yilgör, I.; Yilgör, E.; Wilkes, G. L., Critical parameters in designing segmented polyurethanes and their effect on morphology and properties: A comprehensive review. *Polymer* **2015**, 58, A1-A36.
 15. Jiang, L.; Wu, J.; Nedolisa, C.; Saiani, A.; Assender, H. E., Phase Separation and Crystallization in High Hard Block Content Polyurethane Thin Films. *Macromolecules* **2015**, 48 (15), 5358-5366.
 16. Nozaki, S.; Hirai, T.; Higaki, Y.; Yoshinaga, K.; Kojio, K.; Takahara, A., Effect of chain architecture of polyol with secondary hydroxyl group on aggregation structure and mechanical properties of polyurethane elastomer. *Polymer* **2017**, 116, 423-428.
 17. Aoki, D.; Ajiro, H., Design of polyurethane composed of only hard main chain with oligo (ethylene glycol) units as side chain simultaneously achieved high biocompatible and mechanical properties. *Macromolecules* **2017**, 50 (17), 6529-6538.
 18. Rahmawati, R.; Nozaki, S.; Kojio, K.; Takahara, A.; Shinohara, N.; Yamasaki, S., Microphase-separated structure and mechanical properties of cycloaliphatic diisocyanate-based thiourethane elastomers. *Polym. J.* **2019**, 51 (2), 265-273.
 19. Akbulut, H.; Yoshida, Y.; Yamada, S.; Endo, T., Synthesis and physical properties of poly (urethane) s using vicinal diols derived from acrylate and styrene monomers. *J. Polym. Sci. A. Polym. Chem.* **2019**, 57 (7), 799-805.
 20. Kojio, K.; Nozaki, S.; Takahara, A.; Yamasaki, S., Influence of chemical structure of hard segments on physical properties of polyurethane elastomers: a review. *J. Polym. Res.* **2020**, 27 (6), 1-13.

21. Jiang, L.; Ren, Z.; Liu, W.; Liu, H.; Zhu, C., Synthesis and molecular interaction of Tung oil - based anionic waterborne polyurethane dispersion. *J. Appl. Polym. Sci.* **2020**, *137* (45), 49383.
22. Aoki, D.; Ajiro, H., Clarification of the effects of topological isomers on the mechanical strength of comb polyurethane. *Polym. Chem.* **2021**, *12* (10), 1533-1539.
23. Candau, N.; Stoclet, G.; Tahon, J.-F. o.; Demongeot, A.; Schouwink, P.; Yilgor, E.; Yilgor, I.; Menciloglu, Y. Z.; Oguz, O., Stiff, Strong, Tough, and Highly Stretchable Hydrogels Based on Dual Stimuli-Responsive Semicrystalline Poly (urethane–urea) Copolymers. *ACS Appl. Polym. Mater.* **2021**, *3* (11), 5683-5695.
24. Peng, F.; Yang, X.; Zhu, Y.; Wang, G., Effect of the symmetry of polyether glycols on structure-morphology-property behavior of polyurethane elastomers. *Polymer* **2022**, *239*, 124429.
25. Blundell, D.; Eeckhaut, G.; Fuller, W.; Mahendrasingam, A.; Martin, C., Real time SAXS/stress–strain studies of thermoplastic polyurethanes at large strains. *Polymer* **2002**, *43* (19), 5197-5207.
26. Yeh, F.; Hsiao, B. S.; Sauer, B. B.; Michel, S.; Siesler, H. W., In-situ studies of structure development during deformation of a segmented poly (urethane– urea) elastomer. *Macromolecules* **2003**, *36* (6), 1940-1954.
27. Koerner, H.; Kelley, J. J.; Vaia, R. A., Transient microstructure of low hard segment thermoplastic polyurethane under uniaxial deformation. *Macromolecules* **2008**, *41* (13), 4709-4716.
28. Unsal, E.; Yalcin, B.; Yilgor, I.; Yilgor, E.; Cakmak, M., Real time mechano-optical study on deformation behavior of PTMO/CHDI-based polyetherurethanes under uniaxial extension. *Polymer* **2009**, *50* (19), 4644-4655.
29. Kojio, K.; Matsuo, K.; Motokucho, S.; Yoshinaga, K.; Shimodaira, Y.; Kimura, K., Simultaneous small-angle X-ray scattering/wide-angle X-ray diffraction study of the microdomain structure of polyurethane elastomers during mechanical deformation. *Polym. J.* **2011**, *43* (8), 692-699.
30. Rahmawati, R.; Masuda, S.; Cheng, C.-H.; Nagano, C.; Nozaki, S.; Kamitani, K.; Kojio, K.; Takahara, A.; Shinohara, N.; Mita, K., Investigation of Deformation Behavior of Thiourethane Elastomers Using In Situ X-ray Scattering, Diffraction, and Absorption Methods. *Macromolecules* **2019**, *52* (18), 6825-6833.
31. Higaki, Y.; Suzuki, K.; Ohta, N.; Takahara, A., Strain-induced molecular aggregation states around a crack tip in a segmented polyurethane film under uniaxial stretching. *Polymer* **2017**, *116*, 458-465.
32. Nozaki, S.; Masuda, S.; Cheng, C.-H.; Nagano, C.; Yokomachi, K.; Kamitani, K.; Aoyama, K.; Masunaga, H.; Kojio, K.; Takahara, A., Direct Evaluation of Local Dynamic Viscoelastic Properties of Isotactic Polypropylene Films Based on a Dynamic μ -Beam X-ray Diffraction Method. *ACS Macro Lett.* **2019**, *8* (2), 218-222.
33. Volkersen, O., Die Nietkraftverteilung in zugbeanspruchten Nietverbindungen mit konstanten Laschenquerschnitten. *Luftfahrtforschung* **1938**, *15*, 41-47.

34. Goland, M.; Reissner, E., The stresses in cemented joints. *J. Appl. Mech.* **1944**, *11* (1), A17-A27.
35. Harris, J.; Adams, R., Strength prediction of bonded single lap joints by non-linear finite element methods. *Int. J. Adhes. Adhes.* **1984**, *4* (2), 65-78.
36. Crocombe, A., Global yielding as a failure criterion for bonded joints. *Int. J. Adhes. Adhes.* **1989**, *9* (3), 145-153.
37. Moutrille, M.-P.; Derrien, K.; Baptiste, D.; Balandraud, X.; Grediac, M., Through-thickness strain field measurement in a composite/aluminium adhesive joint. *Compos. Part A Appl. Sci. Manuf.* **2009**, *40* (8), 985-996.
38. Kavdir, E. Ç.; Aydin, M. D., The experimental and numerical study on the mechanical behaviours of adhesively bonded joints. *Compos. B. Eng.* **2020**, *184*, 107725.
39. Laity, P. R.; Taylor, J. E.; Wong, S. S.; Khunkamchoo, P.; Cable, M.; Andrews, G. T.; Johnson, A. F.; Cameron, R. E., Morphological behaviour of thermoplastic polyurethanes during repeated deformation. *Macromol. Mater. Eng.* **2006**, *291* (4), 301-324.
40. Li, X.; Wang, H.; Xiong, B.; Pösel, E.; Eling, B.; Men, Y., Destruction and Reorganization of Physically Cross-Linked Network of Thermoplastic Polyurethane Depending on Its Glass Transition Temperature. *ACS Appl. Polym. Mater.* **2019**, *1* (11), 3074-3083.
41. Tomlin, S.; Ericson, L., Distorted diffractors with special reference to collagen fibres. *Acta Cryst.* **1960**, *13* (5), 395-402.
42. Kasai, N.; Kakudo, M.; Kasai-Kakudo, *X-ray Diffraction by Macromolecules*. Springer: 2005; Vol. 80, 419.
43. Bartczak, Z.; Argon, A.; Cohen, R., Texture evolution in large strain simple shear deformation of high density polyethylene. *Polymer* **1994**, *35* (16), 3427-3441.
44. Xia, Z.-Y.; Sue, H.-J.; Rieker, T., Morphological evolution of poly (ethylene terephthalate) during equal channel angular extrusion process. *Macromolecules* **2000**, *33* (23), 8746-8755.
45. Phillips, A.; Zhu, P.-w.; Edward, G., Simple shear deformation of polypropylene via the equal channel angular extrusion process. *Macromolecules* **2006**, *39* (17), 5796-5803.
46. Bowden, P.; Young, R., Deformation mechanisms in crystalline polymers. *J. Mater. Sci.* **1974**, *9* (12), 2034-2051.
47. He, X., A review of finite element analysis of adhesively bonded joints. *Int. J. Adhes. Adhes.* **2011**, *31* (4), 248-264.